Hindawi
Journal of Nanomaterials
Volume 2017, Article ID 4315905, 11 pages
https://doi.org/10.1155/2017/4315905

Research Article

SnO_2 Nanoparticles Decorated 2D Wavy Hierarchical Carbon Nanowalls with Enhanced Photoelectrochemical Performance

Noor Hamizah Khanis,[1] Richard Ritikos,[1] Wee Siong Chiu,[1] Choon Yian Haw,[2] Nur Maisarah Abdul Rashid,[1] Mei Yuen Chia,[1] Poi Sim Khiew,[3] and Saadah Abdul Rahman[1]

[1]*Low Dimensional Materials Research Centre, Department of Physics, Faculty of Science, University of Malaya, Lembah Pantai, 50603 Kuala Lumpur, Malaysia*
[2]*School of Engineering, Xiamen University Malaysia, Jalan Sunsuria, Bandar Sunsuria, 43900 Sepang, Selangor, Malaysia*
[3]*Faculty of Engineering, University of Nottingham, Malaysia Campus, 43500 Semenyih, Selangor, Malaysia*

Correspondence should be addressed to Noor Hamizah Khanis; hamizahkhanis@gmail.com

Received 31 July 2017; Accepted 16 October 2017; Published 14 November 2017

Academic Editor: Luca Valentini

Two-dimensional carbon nanowall (2D-CNW) structures were prepared by hot wire assisted plasma enhanced chemical vapor deposition (hw-PECVD) system on silicon substrates. Controlled variations in the film structure were observed with increase in applied rf power during deposition which has been established to increase the rate of dissociation of precursor gases. The structural changes resulted in the formation of wavy-like features on the 2D-CNW, thus further enhancing the surface area of the nanostructures. The FESEM results confirmed the morphology transformation and conclusively showed the evolution of the 2D-CNW novel structures while Raman results revealed increase in I_D/I_G ratio indicating increase in the presence of disordered domains due to the presence of open edges on the 2D-CNW structures. Subsequently, the best 2D-CNW based on the morphology and structural properties was functionalized with tin oxide (SnO_2) nanoparticles and used as a working electrode in a photoelectrochemical (PEC) measurement system. Intriguingly, the SnO_2 functionalized 2D-CNW showed enhancement in both Mott-Schottky profiles and LSV properties which suggested that these hierarchical networks showed promising potential application as effective charge-trapping medium in PEC systems.

1. Introduction

Research interests on carbon based nanomaterials from 0D-fullerene, 1D-carbon nanotube (CNT), 2D-carbon nanowall (CNW), and graphene have tremendously increased in the past decades. This is mainly due to the novel properties of carbon based nanostructures such as better conductivity, chemical compatibility, and wide electrochemical stability, in addition to the mechanical and thermal characteristic that are typically exceptional compared to the bulk carbon material [1, 2]. In particular, the study on 2D-carbon nanostructures has bloomed upon the discovery of graphene which has increased the curiosity of researchers on investigating interesting properties shown by nanosystems with graphene-like features.

To date, a plethora of fascinating 2D carbon based nanostructures had been successfully developed such as nanoflakes, nanohorns, nanopetals, and carbon nanowalls. Commonly, most of these 2D nanowalls are composed of few layers of graphene sheets that are loosely stacked together. There are reports claiming that these wall-like carbon nanostructures are actually graphene nanowalls with layers of vertical graphene sheets demonstrating congruent properties [3]. Ma et al. have reported that free standing CNWs possess very high surface area and proved to be an excellent candidate for surface interaction due to the abundance of active reaction sites available compared to that of fully embedded nanowall in horizontal manner [4]. There is also a reported study on free standing nanowalls which are aligned perpendicularly to the substrates surface without requiring auxiliary lateral

support [5]. However, relatively fewer reports are found on 2D-carbon nanowalls (2D-CNWs) grown by hot wire radio frequency assisted plasma enhanced chemical vapor deposition, a physical deposition technique which is known to reproducible and introduces fewer impurities into the film structure.

In this work, the CNW thin films were grown on silicon dioxide substrates using a home-built hw-PECVD at different applied radio frequency (rf) power. The morphology, structural properties, and composition of 2D-CNW thin films were systematically characterized. The novelty of the current study is the ability to fabricate CNWs with free standing wavy structures by hw-PECVD. These nanowalls structures are unique due to the expanded outward feature displaying flaky structures with abundance of active edges. Such features enable these CNWs to serve as matrix for the decoration of SnO_2 nanoparticles to be modified into advanced nanocomposites, which can be employed as a highly reactive active material for photoelectrode application. Photoelectrochemical measurements reflect that these nanocomposites exhibit improved photoelectrochemical properties in contrast to that of its single-component counterpart. To the best of our knowledge, such special hybrid nanocomposite has never been reported yet and hence it may serve as alternative routes for the advancement of nanomaterials research as well as in field of photoelectrochemistry.

2. Materials and Methods

2.1. Synthesis of 2D-CNW Thin Films. A home-built hw-PECVD system (Kejuruteraan Wing Hung, Kuala Lumpur, Malaysia), equipped with a radio frequency source for generating the plasma, was used to fabricate 2D-CNW with Au nanoparticles (Particular GmbH, Burgdorf, Germany) as catalyst. A seven-turn coil of 8 mm diameter made from tungsten wire of 1 mm diameter was used as the hot filament (R. D. Mathis Company, Long Beach, CA, USA). Silicon dioxide (SiO_2) substrates with size of 1×2 cm were placed 10 mm from the filament. The deposition parameters used in the deposition process of the 2D-CNWs are as follows: hydrogen flow rate ratio of methane: 20 : 5 sccm, deposition pressure: 2.15 mbar, substrate temperature: 420°C, hot filament temperature: 1850°C, and deposition time: 35 minutes and the rf power was fixed at 0, 20, 40, 60, 80, and 100 W for the different sets of samples studied in this work.

2.2. Synthesis of SnO_2 Nanoparticles and Deposition of SnO_2-2D CNW. In a typical synthesis process, 9.75 (6.69 g) mmol of tin (II) stearate $Sn(O_2C_{18}H_{35})_2$ (Alfa Aesar Haverhill, MA, USA) was used as organometallic precursor; 4.787 mmol (0.99 g) of 1,2-dodecanediol $C_{12}H_{26}O_2$ (Merck, Kenilworth, NJ, USA) and 195 ml of n-hexadecane, $C_{16}H_{34}$ (Sigma-Aldrich, St. Louis, MO, USA), were subsequently loaded into a 250 mL four-neck round-bottom flask. Under constant magnetic stirring, the mixture was heated to 120°C and saturated under nitrogen blanket for 1 hour. The mixture was then raised to 287°C at 4°C/min of ramping rate and further refluxed for 5 hours. Under vigorous stirring, a change in the solution from clear to pale yellow indicates the formation of SnO_2 nanoparticles. The SnO_2 nanoparticles were directly deposited onto the as-grown 2D-CNW using spin coating method. The SnO_2 nanoparticles were spin-cast at a rotation speed of 3000 rpm during 30 seconds. Then, the sample was annealed at 350°C for 1 hour and rapidly cooled to the room temperature. Two different mass fractions (w%) were used in the preparation of the two nanocomposite samples studied in this work, namely, 2.5 and 5.0 w%.

2.3. Characterization of 2D-CNW and SnO_2 Decorated CNW Thin Films. The as-obtained SnO_2 integrated 2D-CNW films were carefully observed using field emission scanning electron microscope (FESEM) using a FEI Quanta 200 FESEM (FEI Company, Hillsboro, OR, USA). A high resolution transmission electron microscope (HR-TEM, JEM 2100-F) was used to determine the high resolution images of the functionalized nanostructures. The bonding properties of the functionalized 2D-CNW thin films were ascertained by X-ray photoemission spectroscopy (XPS) at the beam line, BL3.2 (a) and (b) of the Synchrotron Light Research Institute in Thailand. The Raman spectra were obtained by using Raman Microscope (Renishaw inVia). The optical properties of the films were measured by UV-Vis-NIR spectrophotometer (Cary 5000, Agilent Technologies). The PEC measurements done on the SnO_2 decorated 2D-CNW thin films were carried out on a three-electrode electrochemical cell system equipped with platinum coil as counter electrode and Ag/AgCl as reference electrode, respectively. Xenon arc lamp (300 W) containing solar mass filter is used as a light source for the PEC system that connected to a potentiostat (PGSTAT204, Metrohm Autolab) to probe the electrical signal generated throughout the irradiation.

3. Results and Discussions

3.1. Formation of Hierarchical 2D-CNW. The FESEM images of the films as a function of different rf power, P_{rf}, are represented in Figure 1. Without applying $P_{rf,}$, one can observe that there is no distinct formation of carbon nanostructures as seen in Figure 1(a). The thermal energy sourced from deposition temperature, whether from the substrate or the hot wire heating, is insufficient to induce the formation of 2D-CNW or any form of film. Notably, it is seen that the formation of nanostructured carbon films began to be observed at P_{rf} as low as 20 W. This implies that plasma power is a vital factor to induce the growth of CNWs which turn out to be an initial stage of nucleation for the development of 2D-CNWs. At this stage, the low decomposition rate could have reduced the number of reactive species such as ion (CH_1^+, CH_2^+, CH_3^+, etc.) and hydrocarbon radicals present in the plasma environment due to the lower kinetic energy of the active species. Moreover, these active species tend to produce high surface energy and eventually agglomerate together before reaching suitable growth sites. When P_{rf} was increased to 40 W, a sharp morphological change is observed and distinct sheet-like 2D-CNWs started to form only at P_{rf} of 60 W which appear to be deposited layer-by-layer forming a larger foam-like matrix covering the entire SiO_2 substrate [6]. These 2D-CNW structures are typically made up of vertical

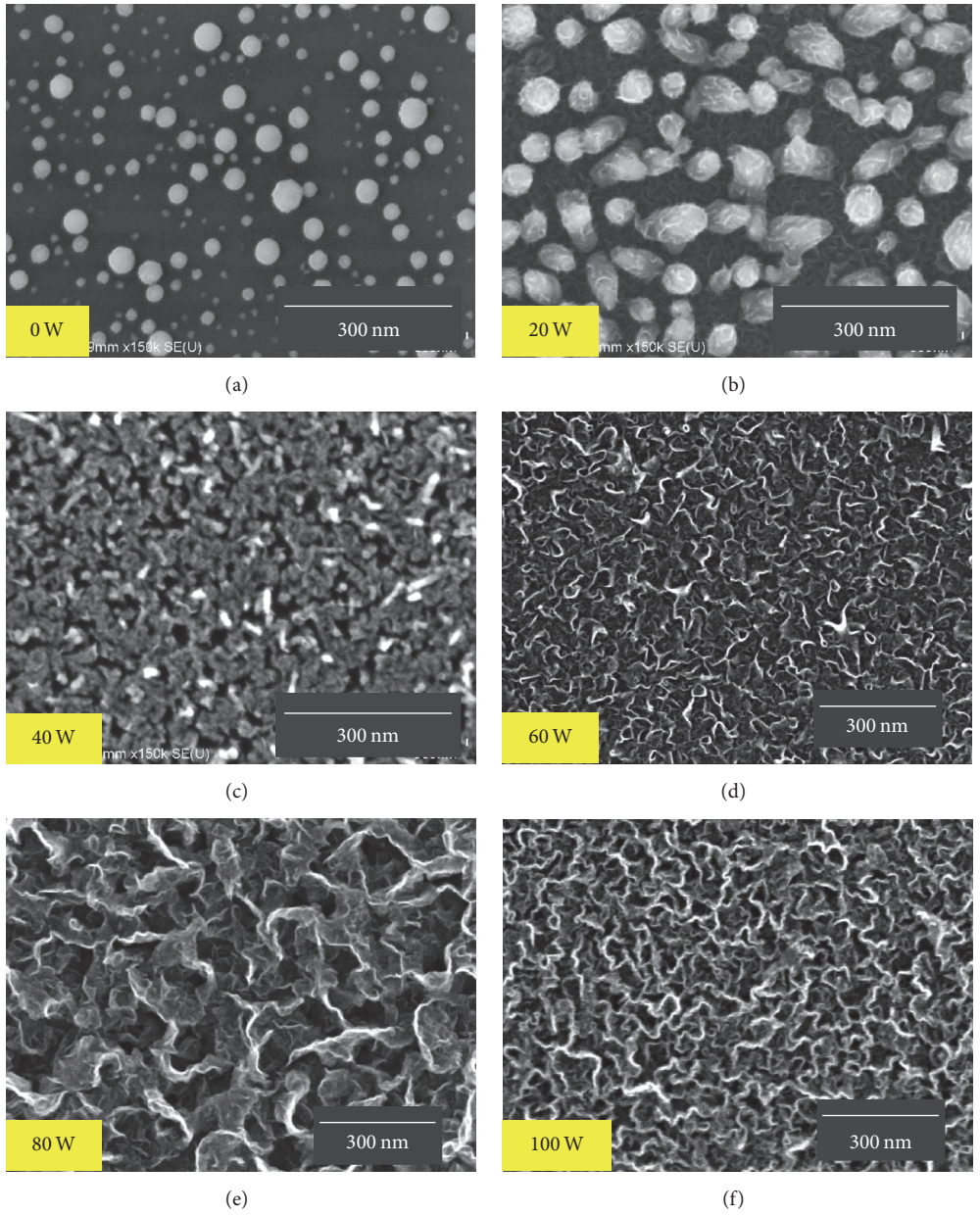

Figure 1: FESEM images of the CNW thin films grown at the applied rf powers of 0 W(a), 20 W (b), 40 W (c), 60 W (d), 80 W (e), and 100 W (f).

sheets with apparent spatial distribution. Conclusively, further increment in P_{rf} could have resulted in the enhancement of momentum, density, and temperature of electrons that facilitated the mobile state of active ions in the gaseous phase and thus increased the active site density for the formation of these novel nanostructures. It can possibly be deduced that the primary and secondary reactions occurring in this system are governed by the decomposition rate of precursor which can influence the formation of various active species in the plasma. The formation of these vertical structures is induced by the effect of local electric field polarity of the plasma resulting from anisotropic polarizability [7, 8]. Further increment of P_{rf} to 80 W renders increase of the wall-to-wall distance and the distribution of the network vertical sheet-like nanostructures as observed in Figure 1(e). At P_{rf} of 100 W, it is deduced that the effective ion bombardment increases the kinetic energy of active species which leads to faster growth rate of secondary wavy-like structures [9]. Such intriguing free standing vertically oriented wall structures offer greater active surface area for materials functionalization, which can provide effective electron pathways and thus can be good candidates as ideal photoelectrode for PEC application.

Figure 2 illustrates a series of magnification TEM views of 2D-CNWs obtained at 80 W. Figure 2(c) demonstrates high resolution TEM image, where the wavy-like 2D-CNW multilayered structures of overlapping plane are clearly visible.

Table 1: FWHM, peak position of D, G, and 2D bands, and I_D/I_G ratio of 2D-CNW thin films.

Rf power (W)	FWHM (cm^{-1})			Peak position (cm^{-1})			I_D/I_G
	D	G	2D	D	G	2D	
0	47.7	45.6	179.4	1348.6	1597.9	2681.9	2.2
20	60.9	55.7	144.2	1354.0	1596.2	2694.1	2.1
40	38.0	51.6	79.2	1353.8	1587.2	2701.6	2.0
60	39.5	46.6	84.8	1353.5	1585.2	2699.3	1.7
80	36.8	37.1	81.5	1350.5	1585.1	2698.1	2.7
100	45.0	54.6	95.6	1352.4	1582.2	2699.9	2.2

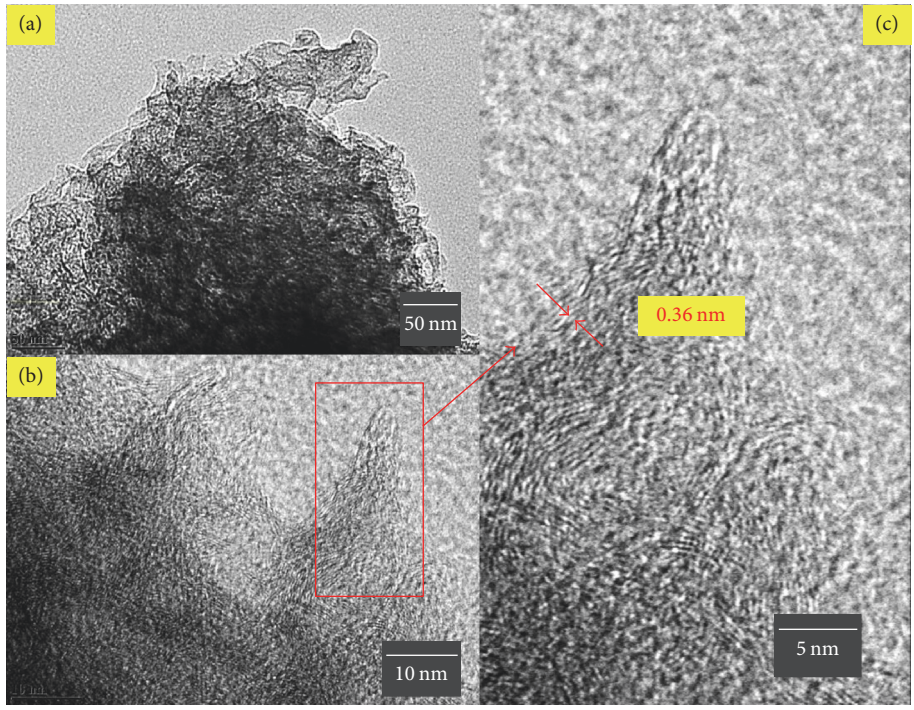

Figure 2: HRTEM images of the CNW prepared at P_{rf} of 80 W.

One may see that the individual layers of the 2D-CNW structures are interconnected to each other to form the wavy-like 2D-CNW with thickness ~10 nm while the measured lattice fringes are about 0.36 nm, which correspond to typical lattice spacing of graphitic materials [10].

Raman spectroscopy was used to characterize the structural properties of the 2D-CNW films prepared at different P_{rf}. Figure 3 shows typical Raman spectra with corrected baseline and the resulting spectra were deconvoluted into six components [11, 12]. The six components are D, G, and 2D bands which were individually deconvoluted by using Lorentzian curve fitting, while D′, D + D′, and D + G bands were deconvoluted via Gaussian curve fitting. The Raman spectra of the as-fabricated thin films reveal four major peaks at around 1350, 1590, 2700, and 2940 cm^{-1} which can be assigned to D, G, 2D, and D + G bands, respectively. The G band is accompanied by a shoulder peak assigned to D′ band at 1620 cm^{-1} while a D + D′ shoulder peak can be found at around 2480 cm^{-1} [9]. The calculated FWHM, peak positions for different bands, and I_D/I_G ratios for the corresponding spectra of the films are summarized in Table 1.

The appearance of G band at around 1590 cm^{-1} is mainly attributed to the stretching vibration mode (E_{2g}) of a hexagonal carbon lattice which confirms the formation of graphitized structure [12]. As reported elsewhere, G peak position for graphitic carbon materials can be seen at around 1580 cm^{-1} [13]. However, the G peak position of the as-fabricated films grown at 0 W and 20 W has been shifted to 1598 and 1596 cm^{-1}, respectively. This shifting and wide $FWHM_G$ suggest that the structures may be due to the indigenousness of nanocrystalline graphitic features of 2D-CNW [14]. Indeed, the corresponding G peak position becomes less prominent as P_{rf} increases which indicates the formation of larger sized graphitic clusters as evidenced from FESEM results.

The strong peak observed at ~1350 cm^{-1} can be assigned to D band which originates from the intervalley double resonance while the presence of D′ band at around 1620 cm^{-1}

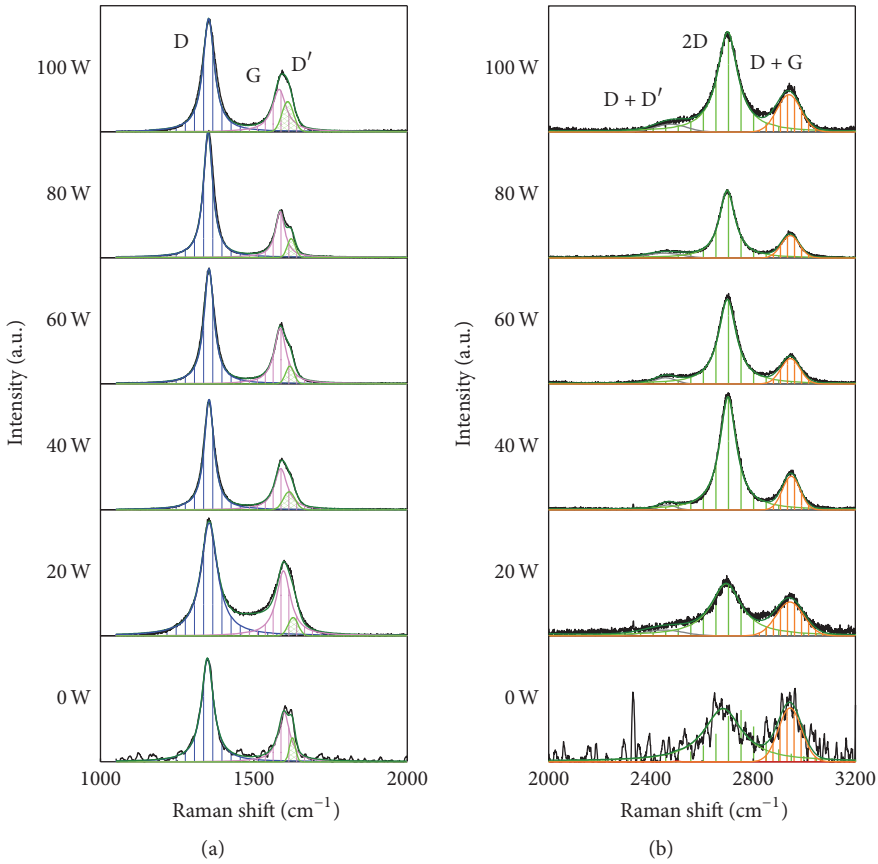

FIGURE 3: Deconvolution of the Raman spectra in the region of (a) 1000–2000 cm^{-1} and (b) 2000–3200 cm^{-1} as function of applied rf power.

is contributed by the intravalley double resonance process. These resonance is produced from the breathing modes of sixfold rings indicating the activation of defects in graphite structure. Such defects include vacancies, strain chain, and/or ring distortion in the 2D-CNW structures. It is worth noting that the large amount of open edges observed on 2D sheets due to the formation of multilayered wall-like structures results in the more prominent intensities of the D peak as compared to the G peak intensities as observed in all the thin films.

The existence of 2D and D + G bands is due to the presence of highly ordered structures with graphene-like domain that gives rise to second-order Raman vibration modes [15]. The presence of 2D band, however, is strongly correlated with the number of layers in the graphene structure [16, 17]. The 2D peak position of 2D-CNW thin films consistently appears at around 2700 cm^{-1} as P_{rf} increased. The large value of $FWHM_{2D}$ indicates that these structures have similar features of the multilayered graphene structures reported by Ferrari and Basko and also confirmed by previously observed HRTEM images [18].

The I_D/I_G value varies in range of 1.7 to 2.7 which is close to the I_D/I_G value of 2D-CNW features previously reported in the literature [9, 19, 20]. This may be due to the enhancement in atomic arrangement as a result of the removal of weak C-C bonds which contribute to the disorder in the film structure. Notably, it is found that the I_D/I_G ratio increases to a maximum of 2.7 at P_{rf} of 80 W but at the same time narrows the FWHM of the G band indicating that there exist two competing mechanisms at this P_{rf}. This suggests that the CNWs prepared at P_{rf} of 80 W consist of small crystallites with relatively high degree of graphitization which correspond well to the study reported by Rout et al. and Kurita et al. [21, 22]. At maximum P_{rf}, I_D/I_G reduced again suggested that the number of ordered structures increased and this is perhaps due to the reduction of defects along the edges of 2D-CNW nanostructures.

The elemental composition of the films was ascertained from XPS measurements. The XPS spectra show the types of bonds are affiliated to the carbon and oxygen atoms present in the films. Narrow scan spectra of C 1s and O 1s as a function of P_{rf} are shown in Figures 4(a) and 4(b), respectively. These two regions represent the binding energy in range of 280–296 eV and 524–540 eV [23]. It appears that the intensity of C 1s peak is appreciably lower for the film prepared without applying P_{rf}. On the other hand, the corresponding O 1s peak intensity is significantly higher compared to films prepared at P_{rf} of 20 to 100 W. These spectra were then deconvoluted by using Gaussian fitting with nonlinear background extraction for further investigation.

As shown in Figure 4(c), the C 1s peak of 2D-CNW thin film prepared at 80 W can be perfectly deconvoluted into

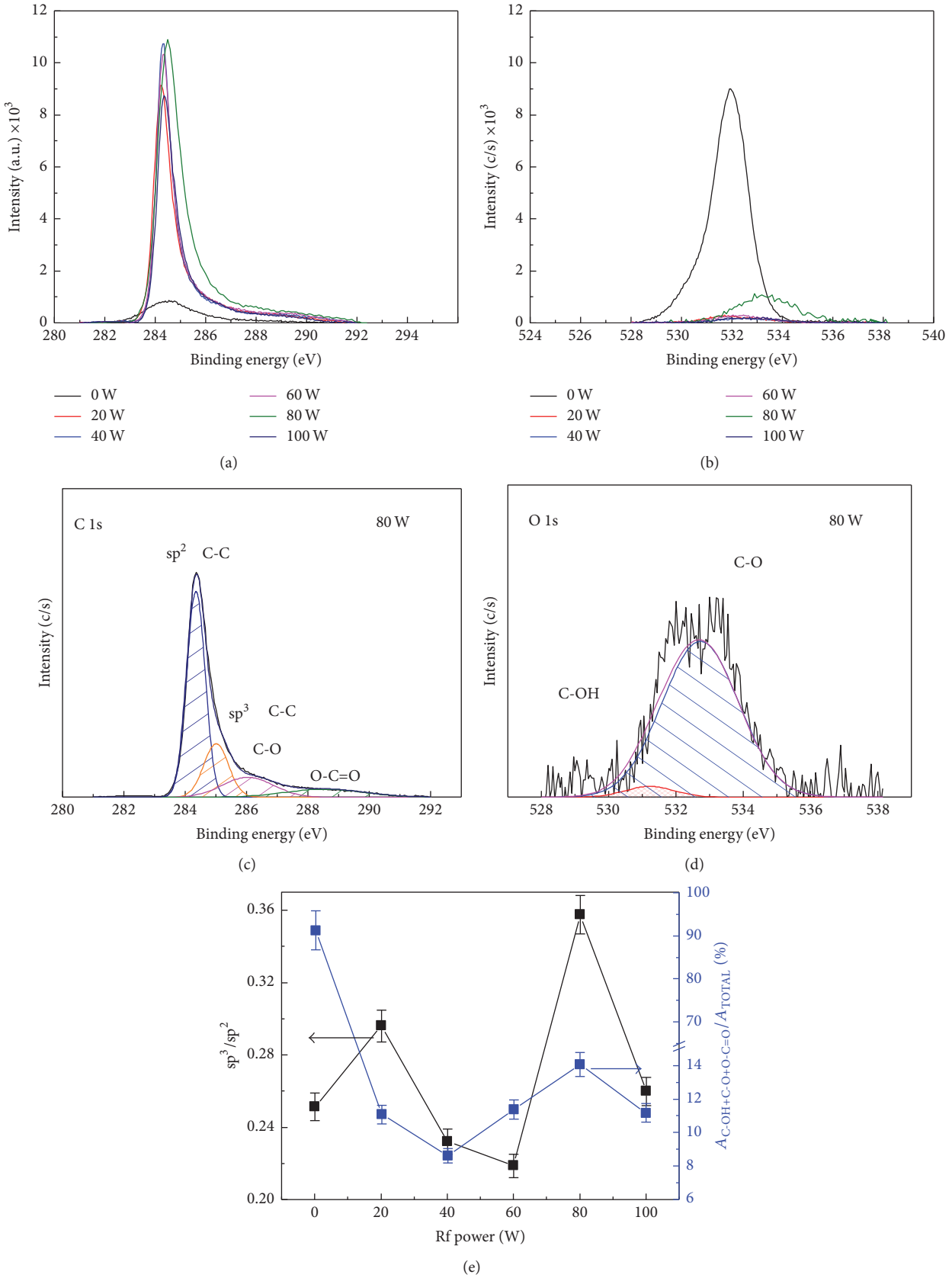

Figure 4: XPS analysis of CNW thin films.

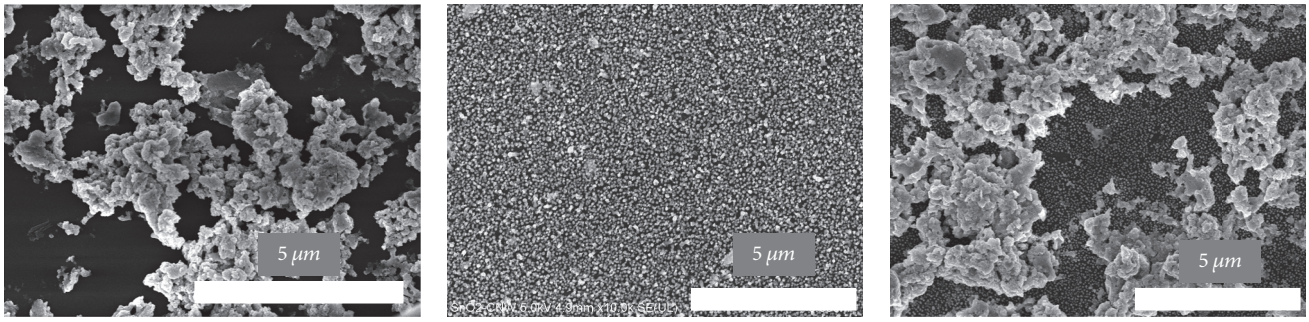

(a) (b) (c)

Figure 5: FESEM image of SnO_2 nanoparticle on bare Si substrate (a) and SnO_2 nanoparticles decorated CNW at 2.5 and 5.0 w% for (b) and (c), respectively.

four separate peaks. The main peak centered at 284.3 eV corresponds to sp^2 C=C, while secondary prominent peak centered at 285.2 eV was assigned to sp^3 C-C. The peaks at 286.5 and 288.7 eV were assigned to C-O and O-C=O, respectively. These binding energies are in agreement with those reported in literature [9, 12, 24]. A similar procedure was utilized to decompose O 1s into two components such as C-OH and C-O bonds as revealed in Figure 4(d). The peak of C-OH and C-O bonds is centered at 531.8 and 533.1 eV, respectively [25]. When the samples were exposed to air, the presence of oxygen not only was associated with the oxygen or water vapor physical absorption on 2D-CNW surface, but also indicates the presence of oxygen atoms that are chemically bonded to the structures [26].

In this work, although the composition appears to be constant throughout the range of P_{rf} applied, further analysis suggests that the difference in the applied power brings about the change in sp^2/sp^3 ratio as a function of P_{rf} as represented in Figure 4(e). Interestingly, the trend shown in sp^3/sp^2 ratio is similar to the Raman I_D/I_G results. The sp^3/sp^2 ratio decreases initially when P_{rf} is increased from 20 W to 60 W and then increases significantly at 80 W. The initial decrease in sp^3/sp^2 ratio supports the earlier suggestion in the Raman results analysis which is attributed to the enhancement in the atomic arrangement. The increase in the number of heterogeneous nucleation sites by reactive H atom in the plasma results in preferential growth of stronger sp^2 C=C bonds in the film. The increase in sp^3/sp^2 for film deposited at P_{rf} of 80 W can be due to the effects produced by the change in the morphology of the film. The increase in defects along the edges of the walls which is significant for these films allows for the preferential formation of sp^3 bonds along these edges. This is supported by the percentage of oxygen related components obtained from analysis of O 1s peak in Figure 4(e).

3.2. Tin Oxide Anchored 2D-CNWs and Photoelectrochemical Measurement. The progression in 2D-CNWs formation from carbon nanostructures at low P_{rf} into 2D-CNWs network structures at higher P_{rf} has been realized in microscopic studies done in the previous section. The growth of CNW thin films (Figure 1) shows that the applied P_{rf} in the 2D-CNWs deposition gives significant influence to their morphological properties. Thus, the choice of P_{rf} for CNW growth is crucial for a study devoted to the fabrication of 2D-CNWs with large wall-to-wall distance network structure suitable for functionalization of SnO_2 nanoparticles for PEC studies. Architecture of semiconductor photoelectrode is of fundamental aspect in the perspective of PEC system performance [27]. Therefore, in this section, 2D-CNWs thin film prepared at 80 W is selected for functionalization of SnO_2 nanoparticles using simple spin coating technique to be used as photoelectrode for PEC measurements.

FESEM image of SnO_2 and SnO_2 nanoparticles functionalized 2D-CNWs (SnO_2-CNWs) thin films is presented in Figure 5. It is observed that the distribution of SnO_2 nanoparticles is not uniform on the smooth surface of SiO_2 bare substrate. Comparatively, it was found that 2.5 w% SnO_2 nanoparticles tend to be distributed uniformly onto 2D-CNWs thin film. This could be due to porosity of the 2D-CNWs covering the c-Si substrate that renders SnO_2 nanoparticles easily incorporated into the CNW matrix. Further functionalization of 5.0 w% SnO_2 nanoparticles on the 2D-CNWs results in agglomeration of SnO_2 on the surface of the CNWs.

The EDX results of 2D-CNW and SnO_2-CNWs thin films are presented in Figure 6(a). These spectra detected C, O, and Si elements on the film with 2D-CNWs and additional Sn element for the SnO_2-CNWs nanocomposite film. Microstructural properties can be realized by the Raman spectra of both 2D-CNWs and SnO_2-CNWs nanocomposite films which are shown in Figure 6(b). The Raman spectrum of CNW thin film reveals four peaks at around 1400, 1590, 2840, and 3030 cm^{-1} assigned to D, G, 2D, and D + G bands, respectively. While SnO_2-CNWs nanocomposite thin film presents three additional peaks at around 358, 475, and 630 cm^{-1} ascribed to E_u, E_g, and A_{1g} Raman active mode of SnO_2 material [28]. Figure 6(c) depicts the reflectance spectra of SnO_2-CNWs nanocomposite thin film deposited at different SnO_2 deposition concentration. Inset in Figure 6(c) shows enlarged 2.5 and 5.0 w% SnO_2-CNWs nanocomposite thin film reflectance spectra. The bandgaps of the as-obtained thin films are further determined from the analysis on the reflectance spectra which are shown in Table 2. The energy

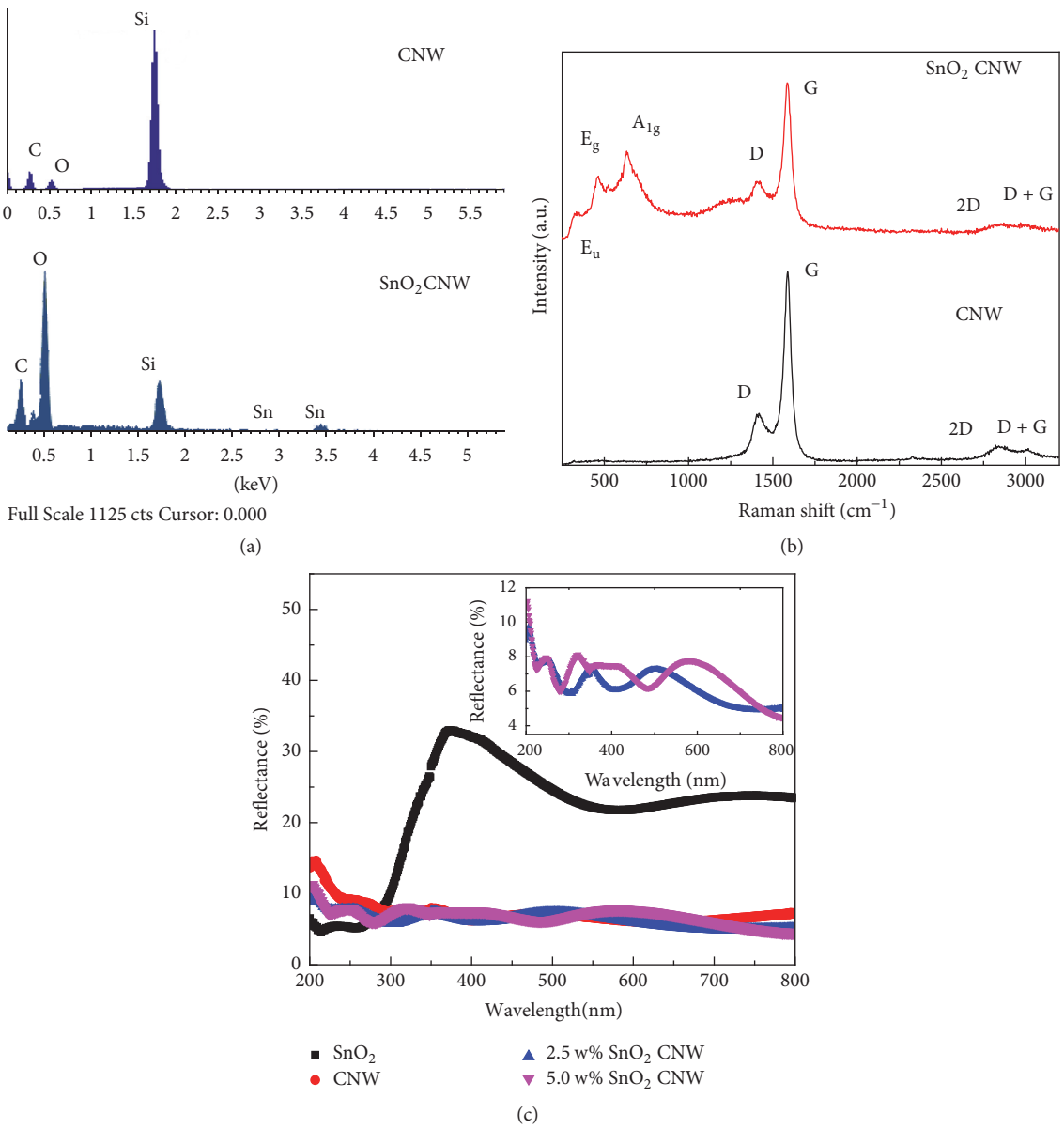

FIGURE 6: (a) EDX spectra of CNW and SnO_2 nanoparticles decorated CNW. (b) Raman spectra of CNW, SnO_2, and SnO_2 nanoparticles decorated CNW. (c) Reflectance spectra of SnO_2 nanoparticles decorated CNW with different concentration.

gaps of CNW and SnO_2 are 1.35 and 3.74 eV, respectively, which is close to the value reported by Kawai et al. [29, 30]. In contrast, the energy gap of the SnO_2-CNWs nanocomposite thin film is found to be in the range of 1.82 to 2.80 eV and the value increases with increase in the concentration of SnO_2 nanoparticles. The combination of both 2D-CNWs and SnO_2 can potentially narrow the bandgap of the SnO_2-CNWs nanocomposite thin film photoelectrode because of electronic interaction between CNWs and SnO_2 that leads to improvement of light harvesting properties of PEC under visible irradiation [31, 32].

In order to evaluate the surface charges for the corresponding films, Mott-Schottky (MS) measurements characteristic plots are illustrated in Figure 7. The donor density of the films can be obtained by using Mott-Schottky equation:

$$\frac{1}{C^2} = \frac{2}{qAN_d\varepsilon\varepsilon_o}\left[V_{\text{bias}} - V_{fb}\frac{KT}{q}\right], \quad (1)$$

where C is the capacitance of the space charge region, q is the elementary electron charge, A is the interfacial area, N_d is donor density of the films, ε is the static dielectric constant of the films, ε_o is the permittivity of free space, V_{bias} is the applied potential, V_{fb} is the flat band potential, K is Boltzmann's constant, and T is the absolute temperature [33]. From the slope in the MS plot N_d for the films are determined as shown in Table 3. The N_d values of SnO_2 and CNW films are almost the same. However, for SnO_2-CNWs nanocomposite

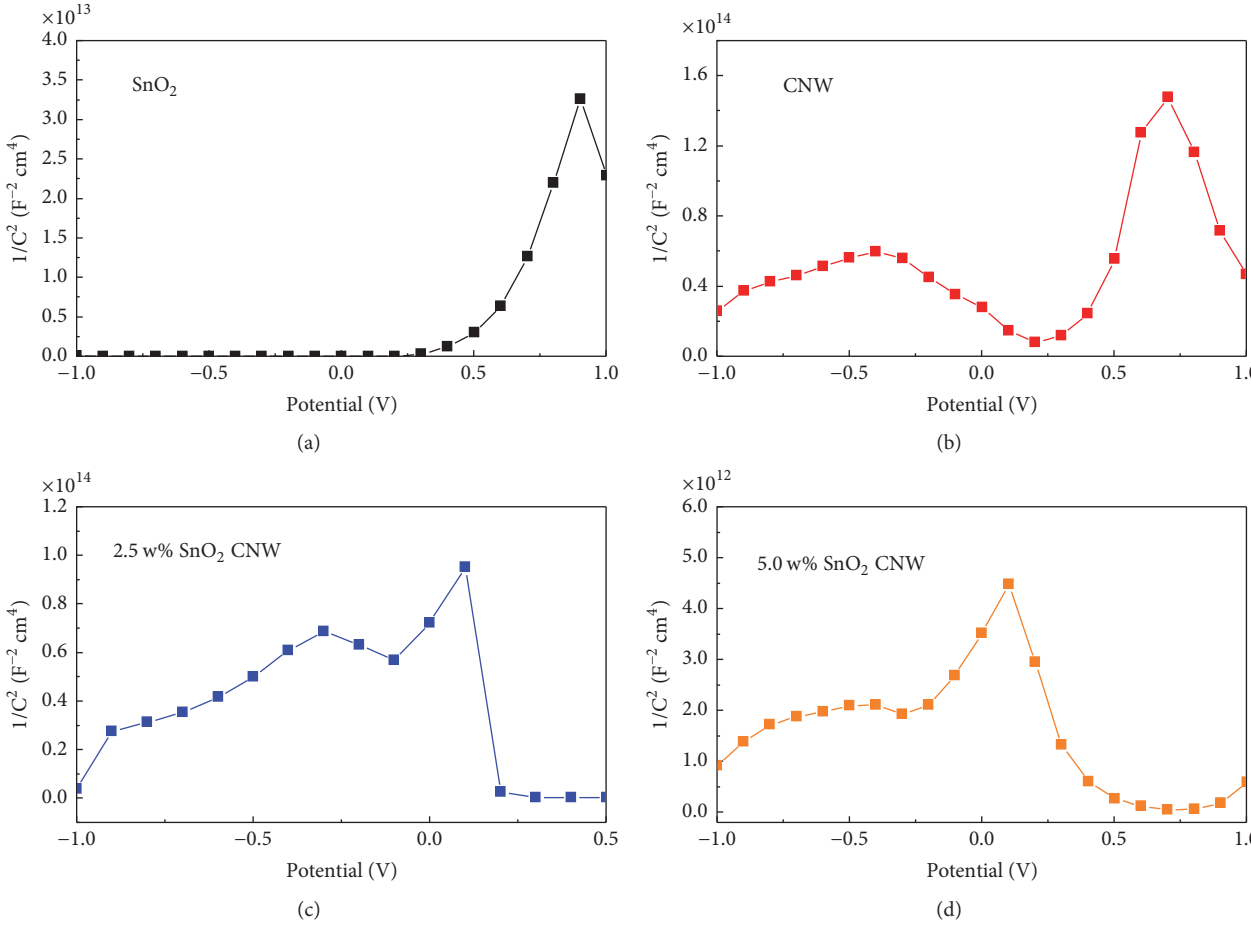

Figure 7: Mott-Schottky plot of the measured capacitance of the SnO_2 (a), CNW (b), and the SnO_2 decorated CNW thin films with SnO_2 concentration of 2.5 w% (c) and 5.0 w% (d).

Table 2: Energy gap of SnO_2, CNW, and SnO_2-CNW thin films.

Sample	Energy gap (eV)
SnO_2	3.74
CNW	1.35
2.5 w% SnO_2-CNW	1.82
5.0 w% SnO_2-CNW	2.06

Table 3: Carrier density N_d of the films.

Sample	Donor density (cm^{-3})
SnO_2	1.16×10^{15}
CNW	2.18×10^{15}
2.5 w% SnO_2-CNW	1.76×10^{16}
5.0 w% SnO_2-CNW	1.30×10^{17}

thin film electrode with SnO_2 concentration of 2.5 w%, the value increases to 1.16×10^{15} cm^{-3} and increases further to 1.30×10^{17} for the film with SnO_2 concentration of 5.0 w%. The key improvement in this case can be attributed to the effective electron transfer between SnO_2 and CNW which in turn improves the conductivity of the photoelectrode [34].

The linear sweep voltammogram (LSV) of the SnO_2, CNW, and the SnO_2-CNWs nanocomposite thin films with SnO_2 concentration of 2.5 and 5.0 w% determined in the presence of 0.1 M Na_2SO_4 without and with illumination are presented in Figures 8(a) and 8(b), respectively. It can be observed that, at positive bias voltage, the anodic current response increases with increase in bias voltage. SnO_2-CNWs nanocomposite thin films with different concentration of 2.5 and 5.0 w% show great enhancement in the anodic current. This may be due to the increase in donor density in the functionalized films. More interestingly, under illumination of simulated solar source on the sample, the anodic current increases for 2.5 and 5.0 w% SnO_2-CNWs nanocomposite thin films. For instance, the current increases from 7.8 mA to 11.8 mA at 1.0 V for 5.0 w% SnO_2-CNWs. Improvement PEC properties of SnO_2-CNWs nanocomposite thin films can be ascribed to the fact that SnO_2 nanoparticles incorporated on wavy-like structures provide larger surface area. The 2D-CNWs network serves as direct route of charge transport which enhance the separation of photogenerated charge carrier which greatly enhanced the PEC response [35]. It is also can be deduced that the density of SnO_2 incorporated

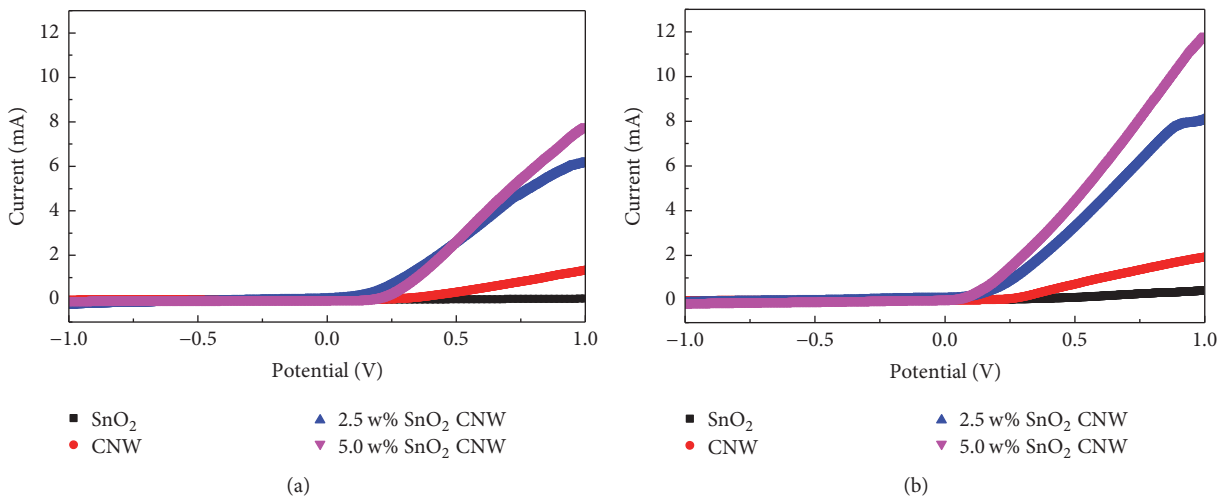

FIGURE 8: Linear sweep voltammograms of the SnO_2, CNW, and the SnO_2 decorated CNW thin films with SnO_2 concentration of 2.5 and 5.0 w% without (a) and under illumination (b).

onto 2D-CNW structures contributes to the enhancement of PEC performance as a result of the increased photon absorption in hybrid materials.

4. Conclusion

In summary, 2D carbon network has been successfully synthesized using a home-built hot wire assisted plasma enhanced chemical vapor deposition system. The rf power applied is shown to modify the morphology of the 2D-CNW structures. The formation of novel graphitic structures was confirmed by Raman spectroscopy and HRTEM analysis. The CNWs were further decorated with SnO_2 nanoparticles employing a simple spin coating technique. From the results, it is anticipated that 2D-CNW structures provide direct pathways of charge transport mitigating recombination of photogenerated electron-hole pairs in the SnO_2 functionalized 2D-CNW thin film. This method could therefore provide a new channel in the preparation of novel carbon nanostructures for advanced hybrid materials that could potentially be used in PEC applications.

Conflicts of Interest

The authors declare no conflicts of interest regarding the publication of this paper.

Acknowledgments

This work was financially supported by Prototype Research Grant Scheme (PRGS: PR003-2016), University of Malaya Research Grant (RG391/17AFR), and Postgraduate Research Fund (PG091/2014A).

References

[1] K. Lehmann, O. Yurchenko, A. Heilemann et al., "High surface hierarchical carbon nanowalls synthesized by plasma deposition using an aromatic precursor," *Carbon*, vol. 118, pp. 578–587, 2017.

[2] T. Itoh, "Synthesis of carbon nanowalls by hot-wire chemical vapor deposition," *Thin Solid Films*, vol. 519, no. 14, pp. 4589–4593, 2011.

[3] B. Kumar, K. Y. Lee, H.-K. Park, S. J. Chae, Y. H. Lee, and S.-W. Kim, "Controlled growth of semiconducting nanowire, nanowall, and hybrid nanostructures on graphene for piezoelectric nanogenerators," *ACS Nano*, vol. 5, no. 5, pp. 4197–4204, 2011.

[4] Y. Ma, H. Jang, S. J. Kim, C. Pang, and H. Chae, "Copper-Assisted Direct Growth of Vertical Graphene Nanosheets on Glass Substrates by Low-Temperature Plasma-Enhanced Chemical Vapour Deposition Process," *Nanoscale Research Letters*, vol. 10, no. 1, article no. 308, 2015.

[5] M. Zhu, J. Wang, R. A. Outlaw, K. Hou, D. M. Manos, and B. C. Holloway, "Synthesis of carbon nanosheets and carbon nanotubes by radio frequency plasma enhanced chemical vapor deposition," *Diamond and Related Materials*, vol. 16, no. 2, pp. 196–201, 2007.

[6] T. Uchida, A. Baliyan, T. Fukuda, Y. Nakajima, and Y. Yoshida, "Charged particle-induced synthesis of carbon nanowalls and characterization," *RSC Advances*, vol. 4, no. 68, pp. 36071–36078, 2014.

[7] Y. Wu and B. Yang, "Effects of Localized Electric Field on the Growth of Carbon Nanowalls," *Nano Letters*, vol. 2, no. 4, pp. 355–359, 2002.

[8] M. Zhu, J. Wang, B. C. Holloway et al., "A mechanism for carbon nanosheet formation," *Carbon*, vol. 45, no. 11, pp. 2229–2234, 2007.

[9] H. J. Cho, H. Kondo, K. Ishikawa, M. Sekine, M. Hiramatsu, and M. Hori, "Density control of carbon nanowalls grown by CH_4/H_2 plasma and their electrical properties," *Carbon*, vol. 68, pp. 380–388, 2014.

[10] H. G. Jain, H. Karacuban, D. Krix, H.-W. Becker, H. Nienhaus, and V. Buck, "Carbon nanowalls deposited by inductively coupled plasma enhanced chemical vapor deposition using aluminum acetylacetonate as precursor," *Carbon*, vol. 49, no. 15, pp. 4987–4995, 2011.

[11] L. Cui, J. Chen, B. Yang, D. Sun, and T. Jiao, "RF-PECVD synthesis of carbon nanowalls and their field emission properties," *Applied Surface Science*, vol. 357, pp. 1–7, 2015.

[12] K. Yu, Z. Bo, G. Lu et al., "Growth of carbon nanowalls at atmospheric pressure for one-step gas sensor fabrication," *Nanoscale Research Letters*, vol. 6, no. 1, pp. X1–9, 2011.

[13] A. Das, B. Chakraborty, and A. K. Sood, "Raman spectroscopy of graphene on different substrates and influence of defects," *Bulletin of Materials Science*, vol. 31, no. 3, pp. 579–584, 2008.

[14] S. K. Jerng, D. S. Yu, Y. S. Kim et al., "Nanocrystalline graphite growth on sapphire by carbon molecular beam epitaxy," *The Journal of Physical Chemistry C*, vol. 115, no. 11, pp. 4491–4494, 2011.

[15] M. A. Pimenta, G. Dresselhaus, M. S. Dresselhaus, L. G. Cançado, A. Jorio, and R. Saito, "Studying disorder in graphite-based systems by Raman spectroscopy," *Physical Chemistry Chemical Physics*, vol. 9, no. 11, pp. 1276–1291, 2007.

[16] M. Hiramatsu, Y. Nihashi, H. Kondo, and M. Hori, "Nucleation control of carbon nanowalls using inductively coupled plasma-enhanced chemical vapor deposition," *Japanese Journal of Applied Physics*, vol. 52, no. 1, Article ID 01AK05, 2013.

[17] X. Song, J. Liu, L. Yu et al., "Direct versatile PECVD growth of graphene nanowalls on multiple substrates," *Materials Letters*, vol. 137, pp. 25–28, 2014.

[18] A. C. Ferrari and D. M. Basko, "Raman spectroscopy as a versatile tool for studying the properties of graphene," *Nature Nanotechnology*, vol. 8, no. 4, pp. 235–246, 2013.

[19] Z. H. Ni, H. M. Fan, Y. P. Feng, Z. X. Shen, B. J. Yang, and Y. H. Wu, "Raman spectroscopic investigation of carbon nanowalls," *The Journal of Chemical Physics*, vol. 124, no. 20, Article ID 204703, 2006.

[20] E. Sandoz-Rosado, W. Page, D. O'Brien et al., "Vertical graphene by plasma-enhanced chemical vapor deposition: Correlation of plasma conditions and growth characteristics," *Journal of Materials Research*, vol. 29, no. 3, pp. 417–425, 2014.

[21] C. S. Rout, A. Kumar, and T. S. Fisher, "Carbon nanowalls amplify the surface-enhanced Raman scattering from Ag nanoparticles," *Nanotechnology*, vol. 22, no. 39, Article ID 395704, 2011.

[22] S. Kurita, A. Yoshimura, H. Kawamoto et al., "Raman spectra of carbon nanowalls grown by plasma-enhanced chemical vapor deposition," *Journal of Applied Physics*, vol. 97, no. 10, Article ID 104320, 2005.

[23] Y. Wang, J. Li, and K. Song, "Study on formation and photoluminescence of carbon nanowalls grown on silicon substrates by hot filament chemical vapor deposition," *Journal of Luminescence*, vol. 149, pp. 258–263, 2014.

[24] H. H. Zou, H. Bai, J. H. Yu et al., "Architecting graphene nanowalls on diamond powder surface," *Composites Part B: Engineering*, vol. 73, pp. 57–60, 2015.

[25] N. Jiang, H. X. Wang, H. Zhang, H. Sasaoka, and K. Nishimura, "Characterization and surface modification of carbon nanowalls," *Journal of Materials Chemistry*, vol. 20, no. 24, pp. 5070–5073, 2010.

[26] Z. González, S. Vizireanu, G. Dinescu, C. Blanco, and R. Santamaría, "Carbon nanowalls thin films as nanostructured electrode materials in vanadium redox flow batteries," *Nano Energy*, vol. 1, no. 6, pp. 833–839, 2012.

[27] M. Zhou, X. W. Lou, and Y. Xie, "Two-dimensional nanosheets for photoelectrochemical water splitting: Possibilities and opportunities," *Nano Today*, vol. 8, no. 6, pp. 598–618, 2013.

[28] C. Haw, W. Chiu, N. H. Khanis et al., "Tin stearate organometallic precursor prepared SnO_2 quantum dots nanopowder for aqueous- and non-aqueous medium photocatalytic hydrogen gas evolution," *Journal of Energy Chemistry*, vol. 25, no. 4, pp. 691–701, 2016.

[29] S. Kawai, S. Kondo, W. Takeuchi, H. Kondo, M. Hiramatsu, and M. Hori, "Optical properties of evolutionary grown layers of carbon nanowalls analyzed by spectroscopic ellipsometry," *Japanese Journal of Applied Physics*, vol. 49, no. 6, pp. 0602201–0602203, 2010.

[30] V. Inderan, S. Y. Lim, T. S. Ong, S. Bastien, N. Braidy, and H. L. Lee, "Synthesis and characterisations of SnO_2 nanorods via low temperature hydrothermal method," *Superlattices and Microstructures*, vol. 88, pp. 396–402, 2015.

[31] X. Chen, Z. Zhang, L. Chi, A. K. Nair, W. Shangguan, and Z. Jiang, "Recent advances in visible-light-driven photoelectrochemical water splitting: Catalyst nanostructures and reaction systems," *Nano-Micro Letters*, vol. 8, no. 1, pp. 1–12, 2016.

[32] J. Xu and M. Shalom, "Electrophoretic Deposition of Carbon Nitride Layers for Photoelectrochemical Applications," *ACS Applied Materials & Interfaces*, vol. 8, no. 20, pp. 13058–13063, 2016.

[33] H. Uchiyama, M. Yukizawa, and H. Kozuka, "Photoelectrochemical properties of Fe_2O_3-SnO_2 films prepared by Sol-Gel method," *The Journal of Physical Chemistry C*, vol. 115, no. 14, pp. 7050–7055, 2011.

[34] K. Xu, N. Li, D. Zeng et al., "Interface bonds determined gas-sensing of SnO_2SnS_2 hybrids to ammonia at room temperature," *ACS Applied Materials & Interfaces*, vol. 7, no. 21, pp. 11359–11368, 2015.

[35] J. Nong and W. Wei, "Direct growth of graphene nanowalls on silica for high-performance photo-electrochemical anode," *Surface Coatings Technology*, vol. 320, pp. 579–583, 2017.